



TWO ROBUST SUPER RESOLUTION APPROACHES IN AEROACOUSTIC IMAGING FOR NEAR-FIELD WIDEBAND EXTENDED SOURCES

Ning *CHU*¹, Ali MOHAMMAD-DJAFARI¹ and José *PICHERAL*²

¹Laboratoire des signaux et systèmes (L2S), CNRS-SUPELEC-PARIS SUD

²Département de Signal et Systèmes Electroniques (SSE), SUPELEC

91192 GIF-SUR-YVETTE, France

ABSTRACT

Recently deconvolution-based methods, like the DAMAS, have greatly improved spatial resolutions of the Beamforming in aeroacoustic imaging. But most of existing methods are not robust to background noise. In this paper, we propose two robust super-resolution approaches using Sparsity Constraint (SC-RDAMAS) and Sparse Regularisation (SR-RDAMAS) respectively to simultaneously estimate source powers and positions, and the variance of background noise. In proposed SC-RDAMAS, sparsity constraint on source power is obtained by considering eigenvalue distributions of observed covariance matrix. When sparsity constraint is hard to determine in strong noise interference, proposed SR-RDAMAS applying ℓ_1 regularisation with proper regularisation parameter can greatly improve resolutions and robustness of proposed SC-RDAMAS. Moreover, proposed SC-RDAMAS can work well even if the source number is over-estimated, but our SR-RDAMAS does not require source number at all. Proposed methods are shown to be robust to noise, wide dynamic range, super resolution and feasibility to use for near-field wideband extended source imaging based on 2D non-uniform microphone array by simulated and wind tunnel data. Our methods are compared with the state-of-art methods: Beamforming, DAMAS, Diagonal Removal DAMAS, DAMAS with sparsity constraint, Covariance Matrix Fitting and CLEAN.

1 INTRODUCTION

Aeroacoustic imaging is a standard technique for mapping the location and strength of aeroacoustic sources with microphone arrays. It provides insight into noise generating mechanisms, which is used for designing quieter vehicles and machinery. In this paper, we aim to investigate near-field wideband aeroacoustic imaging of vehicle surface in wind tunnel test based on the 2D Non-Uniform microphone Array (NUA). State-of-art methods are studied and applied in industry. Beamforming method is fast and simple, but suffers from high sidelobes and its spatial

resolutions are limited especially at low frequencies. Multiple Signal Classification (MUSIC) improves resolutions, but highly depends on the SNR and source number. Though the Near-field Acoustic Hologram (NAH) provides good resolution over entire frequency band, but it is limited by hologram size and can not work well with sparse array. The CLEAN [8] iteratively extracts strong sources from a beamforming image, but it could not separate weak sources from severe background noise. The Deconvolution Approach for Mapping of Acoustic Source (DAMAS) method [2] becomes a breakthrough, but it is sensitive to noise and requires large number of iterations. The DAMAS2 and DAMAS3 accelerate the DAMAS by using invariant point spread function, which inevitably harms resolutions. The ℓ_1 -Singular Value Decomposition (SVD) [4] is proposed to reduce computational complexity and to improve robustness to noise, but it requires the source number to obtain signal subspace. The CMF method with sparsity constraint [11] is robust to noise, but is not feasible to use due to huge dimensionality of variables. Most of classical methods suffers at least one of these drawbacks: poor spatial resolutions, sensitive to background noise, need for source number and high computational cost.

In order to overcome most of these drawbacks, the main idea of proposed approaches is to exploit the sparsity of source spatial distributions. And novelties in this paper are firstly to modify the original DAMAS method to account for background noise, and then introduce sparsity constraint on source power to obtain higher resolutions, and finally apply sparse regularization and select proper regularization parameter to enforce sparsity constraint and obtain super resolutions in poor SNR. The advantages of proposed approach are robust to background noise, super-resolved imaging and applicable to use in wind tunnel experiments with 2D NUA array.

This paper is organized as follows. In Section 2, aeroacoustic imaging formation and its classical inverse solutions are briefly introduced. We then propose the SC-RDAMAS and SR-RDAMAS approaches respectively in Section 3. Section 4 demonstrates performance comparisons on simulated and real data. Finally we conclude the paper in Section 5.

2 FORMULATION OF AEROACOUSTIC IMAGING

2.1 Assumptions

Four necessary assumptions are made: Sources are punctual, temporally uncorrelated; noise is Additive Gaussian White Noise (AGWN), independent and identically distributed (iid); sensors are omnidirectional with unitary gain; and reverberations could be negligible in the anechoic wind tunnel.

2.2 Forward propagation model

Consider M antenna sensors and K near-field wideband sources $\mathbf{s}^* = [s_1^*, \dots, s_K^*]$. And the scanning plane consists of N ($N \gg M > K$) scanning points $\mathbf{s}(f) = [s_1(f), \dots, s_N(f)]^T$ at positions $\mathbf{p} = [p_1, \dots, p_N]^T$ with p_n being 3D coordinate of the point n . Each scanning point could be regarded as a potential source. The total snapshots T_0 measured by each sensor is divided into T segments, where each segment consists of L snapshots. Each segment is then converted into L narrow frequency bins by Fourier Transform. Thus for the segment $i \in [1, T]$ and single frequency $f_i, l \in [1, L]$, the observed vector $\mathbf{z}_i(f_i) = [z_{i1}(f_i), \dots, z_{iM}(f_i)]^T$ at antenna array is modeled:

$$\mathbf{z}_i(f_i) = \mathbf{A}(\mathbf{p}, f_i) \mathbf{s}_i(f_i) + \mathbf{e}_i(f_i) \quad (1)$$

where $\mathbf{e}_i(f_l)$ is AGWN noise vector at antenna array, and $\mathbf{A}(\mathbf{p}, f_l) = [\mathbf{a}(\mathbf{p}_1, f_l), \dots, \mathbf{a}(\mathbf{p}_N, f_l)]$ is $M \times N$ near-field steering matrix, with steering vector:

$$\mathbf{a}(\mathbf{p}_n, f_l) = \left[\frac{1}{r_{n,1}} e^{-j2\pi f_l \tau_{n,1}}, \dots, \frac{1}{r_{n,M}} e^{-j2\pi f_l \tau_{n,M}} \right]^T \quad (2)$$

where $\tau_{m,n}$ is the propagation time from the source n to antenna m , and $r_{n,m}$ is the propagation distance during $\tau_{m,n}$. Actual $r_{n,m}$ and $\tau_{m,n}$ should be corrected according to the refraction in the wind tunnel as discussed in Section 4.

2.3 Classical inverse solutions

Near-field beamforming

For the given location \mathbf{p}_n and single frequency f_l , the steering vector $\mathbf{a}(\mathbf{p}_n, f_l)$ is short as \mathbf{a}_n . An estimate of the source power y_n locating at the scanning point n can be obtained by the beamforming as:

$$y_n = \frac{\tilde{\mathbf{a}}_n^H \hat{\mathbf{R}} \tilde{\mathbf{a}}_n}{\|\tilde{\mathbf{a}}_n\|^2} \quad (3)$$

where operator $(\cdot)^H$ denotes the conjugate transpose; $\|\cdot\|$ is vector norm; and the beamforming coefficient $\tilde{\mathbf{a}}_n$ is:

$$\tilde{\mathbf{a}}_n = [r_{n,1} e^{-j2\pi f_l \tau_{n,1}}, \dots, r_{n,M} e^{-j2\pi f_l \tau_{n,M}}]^T \quad (4)$$

and the estimation of observed covariance matrix \mathbf{R} is $\hat{\mathbf{R}} = \frac{1}{T} \sum_{i=1}^T \mathbf{z}_i(f_l) \mathbf{z}_i(f_l)^H$; and \mathbf{R} is modeled as

$$\mathbf{R} = E\{\mathbf{z}_i(f_l) \mathbf{z}_i(f_l)^H\} = \mathbf{A} \mathbf{X} \mathbf{A}^H + \sigma^2 \mathbf{I} \quad (5)$$

where σ^2 is noise variance; \mathbf{I} is the identical matrix; operator $E\{\cdot\}$ denotes mathematical expectation; and $\mathbf{X} = E\{\mathbf{s} \mathbf{s}^H\}$ is source correlation matrix, with $\mathbf{x} = \text{diag}(\mathbf{X})$ standing for uncorrelated source power vector.

DAMAS [2] and its improved methods

When total snapshot segment is large enough $T \gg 1$, we get $\hat{\mathbf{R}} \approx \mathbf{R}$. By neglecting noise in Eq.(5), the DAMAS [2] method is deduced into:

$$\mathbf{y} = \mathbf{C} \mathbf{x} \quad (6)$$

where $\mathbf{x} = [x_1, \dots, x_N]^T$; $\mathbf{y} = [y_1, \dots, y_N]^T$, and power transferring matrix \mathbf{C} has the coefficient $c_{n,q} = \frac{\|\tilde{\mathbf{a}}_n^H \mathbf{a}_q\|^2}{\|\tilde{\mathbf{a}}_n\|^2}$ with $n, q = 1, \dots, N$, and $c_{nn} = 1$ for any $q = n$. Its iterative non-negative solution is:

$$\hat{x}_n = y_n - \left[\sum_{q=1}^{n-1} c_{nq} \hat{x}_q + \sum_{q=n+1}^N c_{nq} \hat{x}_q \right], \quad \hat{x}_n \geq 0 \quad (7)$$

The DAMAS is a powerful technique to deconvolve the beamforming result and successfully used by the NASA of USA. However, its biggest drawback is not robust to noise pollution. Thus several extended methods have improved the robustness of the DAMAS. Diagonal removal

DAMAS [2] constrains $\text{diag}\{\hat{\mathbf{R}}\} = 0$ to suppress the noise interference, but it harms the weak sources; instead of deconvolving the beamforming result, the CMF with sparsity constraint [11] directly estimates both observed covariance matrix \mathbf{R} and noise variance σ^2 , but its variables matrix are much larger than those of the DAMAS, so the CMF converges much slower.

3 PROPOSED APPROACHES

3.1 Robust DAMAS model

Taking into account of background noise in Eq.(5), we get robust DAMAS model as follows:

$$\mathbf{y} = \mathbf{C}\mathbf{x} + \sigma^2\mathbf{1}_N \quad (8)$$

where $\mathbf{1}_N = \{1, \dots, 1\}_{N \times 1}$. To ameliorate the robustness, noise variance should be estimated. To obtain high resolutions, we apply the sparsity of source spatial distributions: aeroacoustic sources sparsely lay out on the scanning plane, and the source number is much fewer than scanning grids.

3.2 SC-RDAMAS

Based on the robust DAMAS, we propose the SC-RDAMAS approach to solve Eq.(8):

$$\begin{cases} \min_{\mathbf{x}, \sigma^2} \mathcal{J}(\mathbf{x}, \sigma^2) = \|\mathbf{y} - \mathbf{C}\mathbf{x} - \sigma^2\mathbf{1}_N\|_2^2 \\ \text{s.t. } \mathbf{x} \succeq 0, \|\mathbf{x}\|_1 \leq \beta; \quad \sigma^2 \geq 0 \end{cases} \quad (9)$$

Where β represents total source power. If β is too large, the result would be more dispersed than expected; if too small, some weak sources would be lost. A technique [10] to determine β is to normalize each column of the steering matrix \mathbf{A} . So that \mathbf{A} satisfies $\text{diag}(\mathbf{A}^H \mathbf{A}) = \mathbf{1}_N$. Thus total power of uncorrelated sources is $\text{Tr}(\mathbf{X}) = \text{Tr}(\mathbf{X} \mathbf{A}^H \mathbf{A}) = \text{Tr}(\mathbf{A} \mathbf{X} \mathbf{A}^H)$, where $\text{Tr}(\cdot)$ denotes matrix trace. Thus $\beta = \text{Tr}(\mathbf{A} \mathbf{X} \mathbf{A}^H)$ is regarded as total source power. Since \mathbf{R} is Hermitian, \mathbf{R} can be diagonalized into

$$\mathbf{R} = \mathbf{U} \mathbf{\Lambda} \mathbf{U}^H \quad (10)$$

where \mathbf{U} is the unitary matrix, whose columns are eigenvectors of \mathbf{R} , and $\mathbf{\Lambda}$ is a diagonal matrix, whose diagonal values are eigenvalues of \mathbf{R} , with diagonal items $\lambda_1 \geq \lambda_2 \geq \dots \geq \lambda_K \geq \lambda_{K+1} = \dots = \lambda_M = \sigma^2$, where K is the actual source number. According to Eq.(5), we then have

$$\text{Tr}(\mathbf{R}) = \text{Tr}(\mathbf{A} \mathbf{X} \mathbf{A}^H + \sigma^2 \mathbf{I}) = \text{Tr}(\mathbf{U} \mathbf{\Lambda} \mathbf{U}^H) = \text{Tr}(\mathbf{\Lambda}) \quad (11)$$

Thus β is modeled by

$$\beta = \text{Tr}(\mathbf{A} \mathbf{X} \mathbf{A}^H) = \text{Tr}(\mathbf{\Lambda} - \sigma^2 \mathbf{I}) \quad (12)$$

In practice, β is estimated by

$$\hat{\beta} = \text{Tr}(\hat{\mathbf{\Lambda}} - \hat{\sigma}^2 \mathbf{I}) \quad (13)$$

where $\hat{\Lambda}$ is defined by $\hat{\mathbf{R}} = \hat{\mathbf{U}}\hat{\Lambda}\hat{\mathbf{U}}^H$. For simplicity, $\hat{\sigma}^2 = \min\{\lambda_m, m = 1, \dots, M\}$ [10]; for a better initialization [11],

$$\hat{\sigma}^2 = \frac{1}{M - \hat{K}} \sum_{m=\hat{K}+1}^M \lambda_m \quad (14)$$

where \hat{K} is the estimated source number.

In proposed SC-RDAMAS approach, we apply the property of eigenvalue distribution to estimate K . Let $\lambda(m)$ with $m = 1, \dots, M$ denote the eigenvalue distribution of \mathbf{R} , defined by the M diagonal items of Λ , with $\lambda_1 \geq \lambda_2 \geq \dots \geq \lambda_K \geq \lambda_{K+1} = \dots = \lambda_M = \sigma^2$. Since $\lambda(m)$ is a non-increasing function, the second-order derivative $d''\lambda(m)$ describes the change of decreasing rate of $\lambda(m)$. From certain point \hat{K} , the change approaches zero ($d''\lambda(\hat{K}) \approx 0$). Thus \hat{K} can be regarded as the estimation of K . This conclusion could be explained by the sparsity fact that Λ has much fewer number of source powers ($2KIM \ll N$) than that of noise powers who are not greatly distinct from each other (for AWGN noise, noise power is the same); therefore the curve of eigenvalue distribution has a short and steep head, and a long and smooth tail, which are illustrated in Fig.1 for simulated and real data respectively. Figure 2a reveals the influence of estimated source number in proposed SC-RDAMAS. Under-estimation of source number ($\hat{K} < 9$) significantly affects the power image reconstruction error δ_2 , but over-estimation ($\hat{K} > 13$) does not affect at all, since proposed SC-RDAMAS can estimate the noise variance and make δ_2 relatively small.

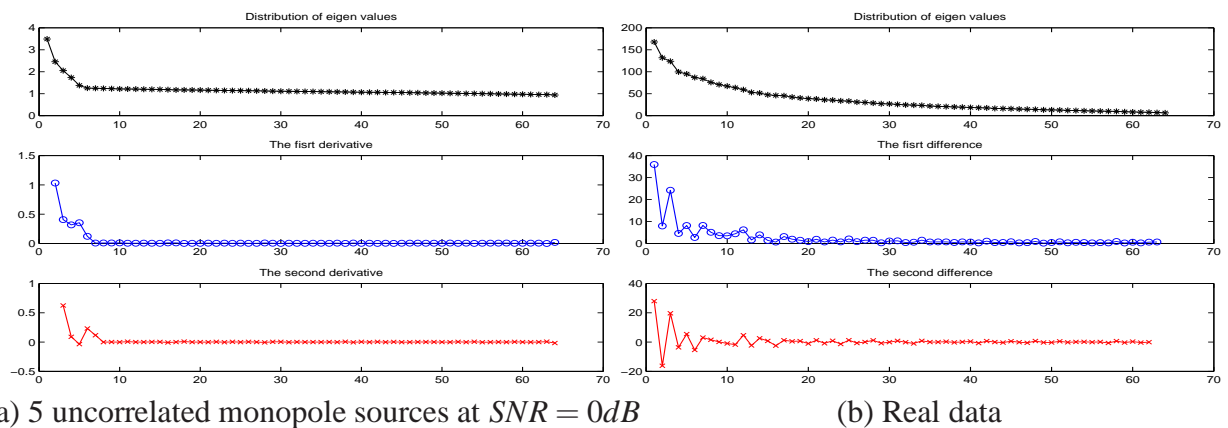


Figure 1: Eigenvalue distribution $\lambda(m)$, first-order ($-d'\lambda(m)$) and second-order ($-d''\lambda(m)$) derivatives (from ceiling to bottom) at 2500Hz, y-axis $\lambda(m)$, x-axis $m = 1, \dots, M$.

3.3 SR-RDAMAS

In very poor SNR cases, sparsity constraint (β) is not easily to determine according to Eq.(13). To enforce the sparsity constraint, proposed SR-RDAMAS approach combines ℓ_1 regularization with the Least Mean Square (LMS) criterion as follows:

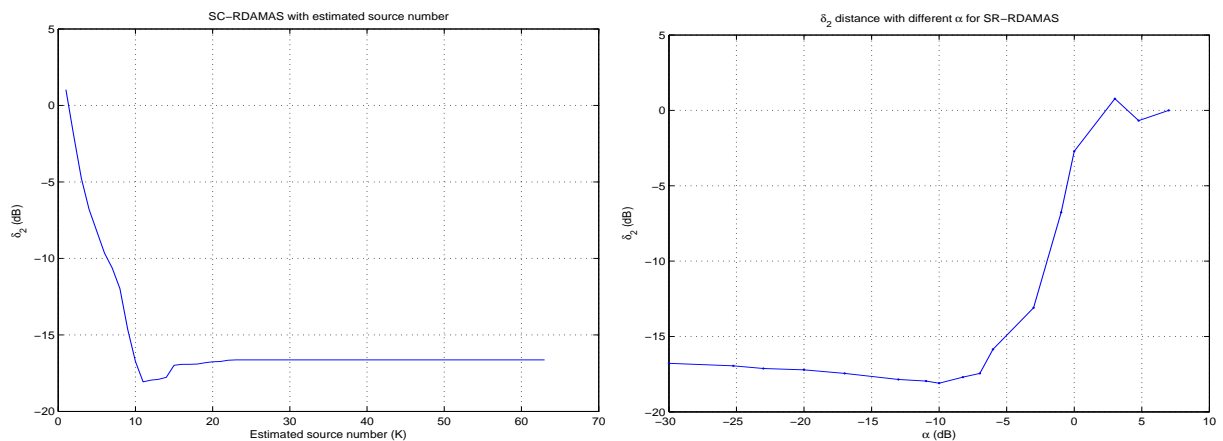
$$\begin{cases} \min_{\mathbf{x}, \sigma^2} \mathcal{J}(\mathbf{x}, \sigma^2) = \|\mathbf{y} - \mathbf{C}\mathbf{x} - \sigma^2\mathbf{1}_N\|^2 + \alpha\|\mathbf{x}\|_1 \\ \text{s.t. } \mathbf{x} \succeq 0; \quad \sigma^2 \geq 0 \end{cases} \quad (15)$$

In Eq.(15), the ℓ_1 regularization offers more information of sparse distribution prior than the sparsity constraint in Eq.(9) of proposed SC-RDAMAS, especially when the forward model of Eq.(8) is severely interfered by noises. Proposed SR-RDAMAS approach offers the iterative non-negative LMS solutions with ℓ_1 -norm regularization for the system of linear equations. The associated inverse algorithm is a convex quadratic program which can be solved efficiently.

For regularization parameter, α is selected by using Bayesian interpretation. The paper [5] argued that α should be proportional to the inverse of the SNR. And [3] indicated that $\alpha = \sigma \sqrt{2 \log(M)}$ with M being the number of antenna. In proposed SR-RDAMAS, α is selected by minimizing the power image reconstruction error δ_2 as follows:

$$\alpha = \arg \min_{\alpha} \delta_2(\alpha) \quad (16)$$

where $\delta_2(\alpha) = \|\hat{x}(\alpha) - x\|_2^2 / \|x\|_2^2$ is relative error of power image reconstruction between original image x and estimated image \hat{x} . And δ_2 measures the estimation performances and sparsity state. In Fig.2b, $\alpha \in [-10, -5]dB$ ($[0.1, 0.3]$) is a proper value region for the proposed SR-RDAMAS, and since proposed SR-DAMAS can well estimate noise variance, δ_2 is relatively small even when small value of α is selected. Moreover, source number in proposed SR-RDAMAS is not necessary any more as proposed SC-RDAMAS.



(a) δ_2 VS \hat{K} ($K \in [9, 13]$) in proposed SC-RDAMAS. (b) δ_2 VS α in proposed SR-RDAMAS.

Figure 2: Source number estimation \hat{K} in proposed SC-RDAMAS and selection of regularization parameter α in proposed SR-RDAMAS based on simulations in Section 4

Both proposed SC-RDAMAS in Eq.(9) and SR-RDAMAS in Eq.(15) are the convex quadratic minimization under linear matrix constraints, which can be solved by interior point methods using MATLAB toolbox SeMuDi [9].

3.4 Wideband estimation

In wind tunnel experiment, aeroacoustic sources are generated by frictions between the vehicle and wind flow. Physically, different vehicle parts produce vibrations with different frequencies. Therefore aeroacoustic sources are near-field wideband signals. Consider the frequency range

$[f_{min}, f_{max}]$ consisting of L frequency bins. Let $\hat{x}(f_l)$ be the estimation of $x(f_l)$ in l th frequency bin. Then source powers x_{wb} over wideband $[f_{min}, f_{max}]$ can be estimated by

$$\hat{x}_{wb} = \frac{1}{L} \sum_{f_l=f_{min}}^{f_{max}} \hat{x}(f_l) \quad (17)$$

4 SIMULATIONS AND REAL DATA

In this section, our proposed approaches are compared with some of the state-of-art methods for near-field wideband extended sources imaging on simulated and real data respectively. The simulations and experiments use the same configurations as follow. There are 64 2D NUA array on vertical plane, whose averaging array aperture is $d = 2m$ with longer horizontal aperture, as shown in Fig.3a. For NUA array, it yields almost the same performance as the uniform array with more sensors does as discussed in [6]. The distance between source plane and array is around $R = 4.50m$, thus the beamforming resolution at $f = 2500Hz$ is $\Delta B \approx \lambda R/d = 31cm$. For scanning step, we choose $\Delta x = 5cm$ to satisfy $\Delta x/\Delta B < 0.2$ for any $f < 3500Hz$, which avoids the spatial aliasing in the DAMAS [2]. The propagation speed is $c_0 \approx 340m/s$. Results are illustrated by decibel (dB) images and section profiles.

4.1 Extended sources

An aeroacoustic monopole is the source who radiates isotropically in all directions. Any source whose dimensions are much smaller than its wavelength will act as a monopole. An extended source is loosely defined as a source consisting of some spatially separated and temporally uncorrelated monopoles. In contrast, a coherent source is made up of correlated monopoles who have a constant phase difference between each other. Though coherent sources are the ideal model to simulate real directivity patterns, it is time-consuming to estimate both source amplitudes and positions, as well as the correlation function as discussed in [1]. Therefore, extended sources with various patterns are used to simulate directivity patterns of actual sources.

4.2 Simulations

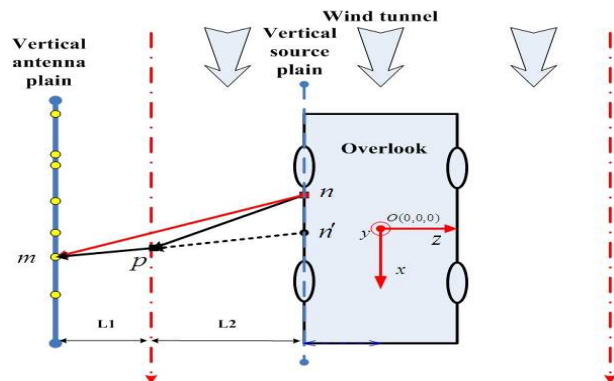
On simulations, the scanning region is $85 \times 135cm^2$ and there are $T_0 = 10000$ snapshots at the array. In Fig.4a, there are 4 monopoles and 5 extended sources with different patterns; their powers are $0.08 \sim 2$ ($-10.27dB \sim 3.7dB$) with $14dB$ dynamic range. The noise is $\sigma^2 = 0.85$ ($-0.7dB$), and averaging $SNR = 0dB$.

The results are shown in Fig.4. The Beamforming just gives few strong sources, since its resolution at $f = 2500Hz$ is $\Delta B \approx \lambda R/d = 31cm$. The DAMAS and SC-DAMAS are sensitive to the noise. The DR-DAMAS eliminates the noise interference and well estimate the extended source, but fails to detect weak monopole sources. The CMF well estimates the noise variance, and obtains better spatial resolutions. However, it loses some of weak sources, and does not well reconstruct the extended sources. The proposed SC-RDAMAS and SR-RDAMAS work much better than the above methods. They not only better estimate the noise variance, but also better estimate positions and powers of all monopoles and extended sources. From Table 1

and 2, averaging estimation error $\overline{\Delta x^*}$ clearly shows that our SC-RDAMAS and SR-RDAMAS approach outperform mentioned classical methods.



(a) Wind tunnel S2A [7].



(b) Overlook and wind tunnel effect.

Figure 3: Configurations of wind tunnel S2A.

Table 1: Power estimation of monopoles and averaging estimation error $\overline{\Delta x^*} = \frac{1}{K} \sum_{k=1}^K |x_k^* - \hat{x}_k^*|$ with real source power $\mathbf{x}^* = \text{diag}\{E[\mathbf{s}^{*H} \mathbf{s}^*]\}$.

Source powers	0.08	0.18	0.98	0.50	$\overline{\Delta x^*}$	δ_2
Beamforming	1.57	11.28	3.51	2.02	4.16	121.93
DAMAS	0	0	0	0	0.44	1.33
SC-DAMAS	0	0	0	0.65	0.35	0.51
DR-DAMAS	0	0	0.77	0.23	0.19	0.10
CMF	0.09	0	0.80	0.40	0.12	0.04
SC-RDAMAS	0.09	0.10	1.05	0.43	0.06	0.02
SR-RDAMAS	0.08	0.13	0.94	0.45	0.05	0.015

4.3 Real data

Figure 3 shows configurations of wind tunnel S2A [7]. The scanning region is $135 \times 470 \text{cm}^2$. There are $T_0 = 524288$ snapshots, $T = 204$ segments. Wideband is $2400 \text{Hz} - 2600 \text{Hz}$ with $B = 21$ frequency bins. The results are shown by normalized dB images with 10dB span. For corrections of propagation time $\tau_{n,m}$ and distance $r_{n,m}$, we apply equivalent source that antenna m seems to receive the signal from equivalent source n' along a direct line $d_{n',m}$ during the same propagation time $\tau_{n',m}$, as if there is no wind influence, as shown in Fig.3b.

For regularization parameter selection in proposed SR-RDAMAS on real data, we use hybrid data by adding synthetic sources to the real data, then regularization parameter is determined according to Eq.(16). Five synthetic extended sources with different patterns are generated as seen in the Fig.5a, whose total powers are from -4.5dB to 0dB .

Table 2: Power estimation of extended source, SNR = 0dB.

Source powers	2.00	2.00	2.00	2.00	2.00	2.00	$\Delta\lambda^*$
Beamforming	2.64	9.60	9.70	9.64	11.34	9.77	6.78
DAMAS	4.50	1.25	0.48	2.54	0.49	1.88	1.15
DR-DAMAS	2.15	2.05	1.82	1.83	2.50	1.45	0.27
SC-DAMAS	2.29	0.66	2.75	2.06	0.86	2.34	0.65
CMF	1.36	2.86	2.07	2.09	1.92	1.05	0.45
SC-RDAMAS	1.83	2.00	2.05	1.72	2.16	1.95	0.12
SR-RDAMAS	1.94	1.99	1.98	1.76	2.10	1.91	0.09

For aeroacoustic imaging on the car side, the Fig.5 illustrates the normalized estimated power images of various methods at 2500Hz with the span 10dB. The beamforming merely gives the fuzzy image of strong sources around the front wheel, the rearview mirror and the back wheel, as seen in Fig.5b; in Fig.5c, the DAMAS well deconvolves the beamforming image, and discovers weak sources on the front light, front cover, the top antenna and side windows; however it also gets many false targets on the air; the DR-DAMAS eliminates most of the false targets, but it also harms weak sources, as shown in Fig.5d; the Fig.5e shows that the CLEAN overcomes drawbacks of the DAMAS, but unexpected strong points are detected on the ground; in contrast, the proposed SC-RDAMAS not only suppress the noise interference and obtain more precise positions and power levels than the above methods, but also discovers all the strong sources and most of the weak sources, as demonstrated in Fig.5f; since the sparsity constraint is determined by real source number $\hat{K} = 20$ as seen in Fig.1b, Figure 5g shows the acceptable result obtained by SC-RDAMAS on real data ; finally, the Fig.5h reveals that our SR-RDAMAS achieves the best performance of all for synthetic source estimations and the noise suppression on the profiles of wheels and mirrors; and proposed SR-RDAMAS also removes most of the false targets under the cars and on the air; the regularization parameter is selected as $\alpha = 0.1$ according to the Eq.(16) with the help of synthetic sources. Therefore Fig.5i gives an expected result achieved by proposed SR-RDAMAS on real data.

Wideband data

Based on the effectiveness and feasibility at single frequency, we compare the proposed approaches with the DR-DAMAS and the CLEAN for the near-field wideband data of 2400 – 2600Hz, as Fig.6 illustrated. Each method obtains a better result than the correspondent one at 2500Hz in Fig.5, since the real sources are enforced and the flashing false targets are suppressed over the wideband average. The estimations of the DR-DAMAS in Fig.6a are reasonable and acceptable, but the spatial resolutions are not high enough on the front wheel and rearview mirror; Fig.6b shows that the CLEAN greatly ameliorates the resolutions, but holds some unexpected points under the car body; the proposed SC-RDAMAS in Fig.6c has the advantages of the CLEAN, and it gets wide dynamic range of source powers around the front wheel, but not sparse enough; finally, our SR-RDAMAS in Fig.6d enforces the sparse state and extracts more accurate source positions and powers, both for the strong sources around the front wheel and

the weak ones on the mirror and back wheel.

5 CONCLUSION

In this paper, we propose two robust super-resolution approaches with sparsity constraint (SC-RDAMAS) and sparse regularization (SR-RDAMAS) for near-field wideband aeroacoustic extended source imaging in poor SNR situations. We firstly modify the original DAMAS method to account for background noise, and then introduce sparsity constraint on source power to obtain higher resolutions, and finally apply sparse regularization and select proper regularization parameter to enforce sparsity constraint and obtain super resolutions in poor SNR. In the proposed SC-RDAMAS, sparsity constraint on source power is applied by using the eigenvalue distributions; based on the SC-RDAMAS, proposed SR-RDAMAS applies the ℓ_1 regularization with selection of regularization parameter to enforce the sparse constraint and achieve super spatial resolution. Moreover, proposed SC-RDAMAS can work well even if the source number is over-estimated, but our SR-RDAMAS does not require source number at all. The advantages of our method are robust to noise interference, wide dynamic range of estimated powers, super spatial resolutions and feasible to use in the wind tunnel tests based on 2D non-uniform microphone antenna array. The effectiveness and feasibility of proposed methods are verified by comparison with the state-of-art methods: the Beamforming, DAMAS, DR-DAMAS, SC-DAMAS, CMF and CLEAN. Our methods are applicable in the monopole and extended source imaging on simulated and real data offered by Renault SAS. To select sparser priors and adaptively estimate hyper-parameter (forward model parameters, prior model parameters etc.), we are investigating a Bayesian inference approach.

6 ACKNOWLEDGEMENT

The authors would like to gratefully thank Renault SAS for offering the real data for our researches.

References

- [1] D. Blacodon. “Combustion-Noise Characterization of a Turbofan Engine with a Spectral Estimation Method.” *Journal of Propulsion and Power* 2009, 25(2), 374–379, 2009.
- [2] T. Brooks and W. Humphreys. “A deconvolution approach for the mapping of acoustic sources (DAMAS) determined from phased microphone arrays.” *Journal of Sound and Vibration*, 294(4-5), 856–879, 2006. ISSN 0022-460X.
- [3] S. Chen, D. Donoho, and M. Saunders. “Atomic decomposition by basis pursuit.” *SIAM journal on scientific computing*, 20(1), 33–61, 1999.
- [4] D. M. et al. “A sparse signal reconstruction perspective for source localization with sensor arrays.” *IEEE Transactions on Signal Processing*, 53(8), 3010–3022, 2005.
- [5] J. Fuchs. “Multipath time-delay detection and estimation.” *Signal Processing, IEEE Transactions on*, 47(1), 237–243, 1999.

- [6] C. E. Kassis, J. Picheral, and C. Mokbel. “Advantages of nonuniform arrays using root-music.” *Signal Processing*, pages 689–695, 2010.
- [7] A. Menoret, N. Gorilliot, and J.-L. Adam. “Imagerie acoustique en soufflerie S2A.” In *10ème Congrès Français d’Acoustique* (edited by S. F. d’Acoustique SFA). Lyon, France, 2010.
- [8] P. Sijtsma. “Clean based on spatial source coherence.” *International Journal of Aeroacoustics*, 6(4), 357–374, 2007.
- [9] J. F. Sturm. “Using sedumi 1.02, a matlab toolbox for optimization over symmetric cones.”, 1998.
- [10] T. Yardibi, J. Li, P. Stoica, and L. Cattafesta III. “Sparsity constrained deconvolution approaches for acoustic source mapping.” *The Journal of the Acoustical Society of America*, 123, 2631, 2008.
- [11] T. Yardibi, J. Li, P. Stoica, N. S. Zawodny, and L. N. Cattafesta. “A covariance fitting approach for correlated acoustic source mapping.” *Journal of The Acoustical Society of America*, 127, 2010.

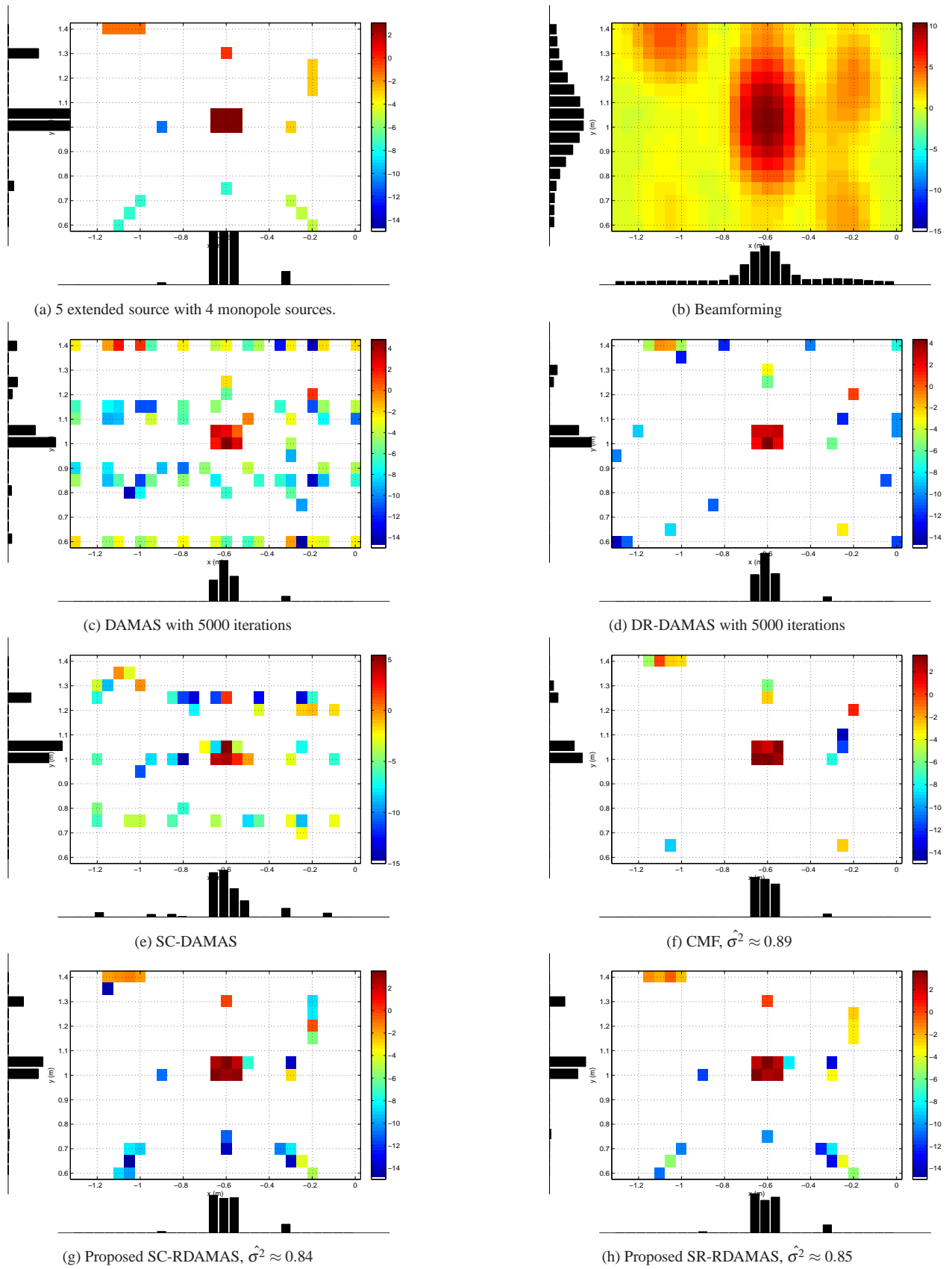
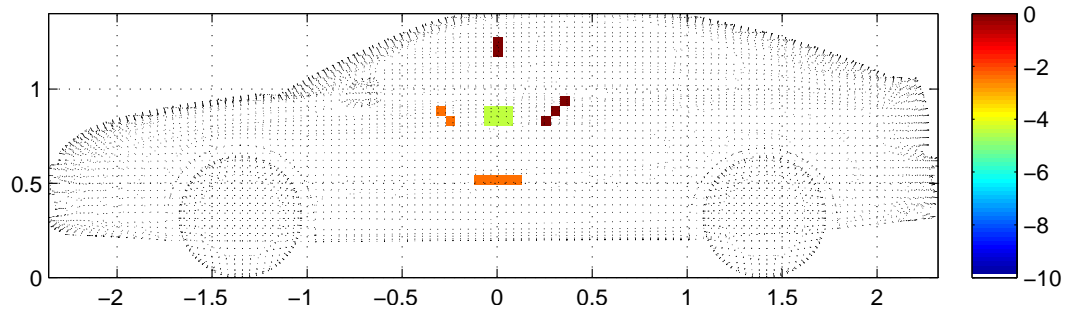
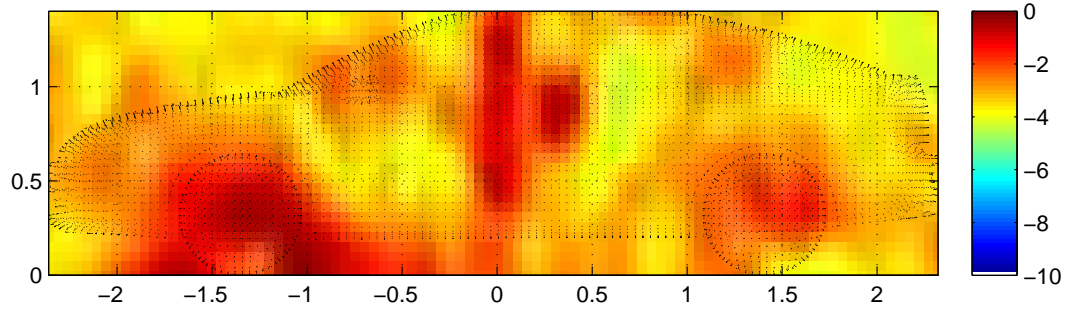


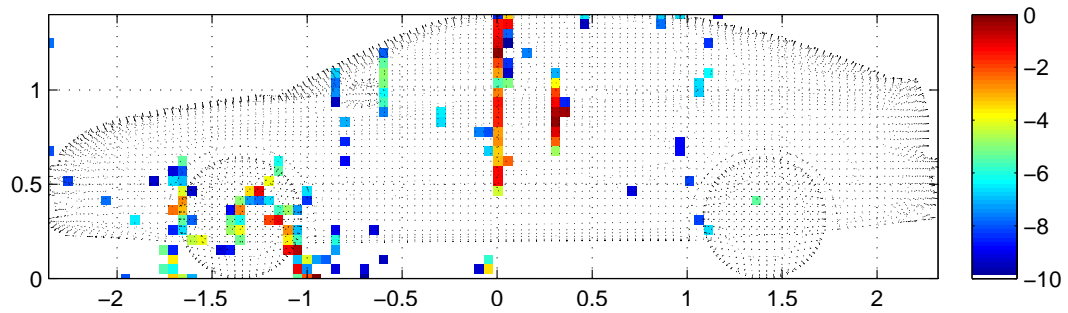
Figure 4: Simulation on extended sources, real $\sigma^2 = 0.85$, SNR = 0 dB, imaging at 2500Hz.



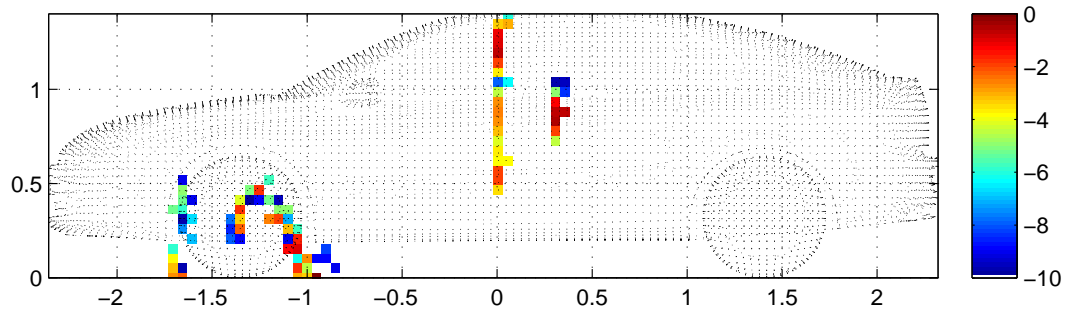
(a) Synthetic sources with different forms.



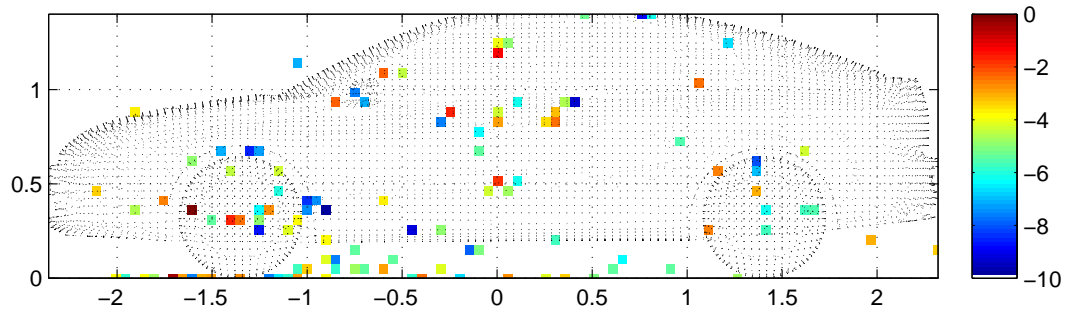
(b) Beamforming on hybrid data.



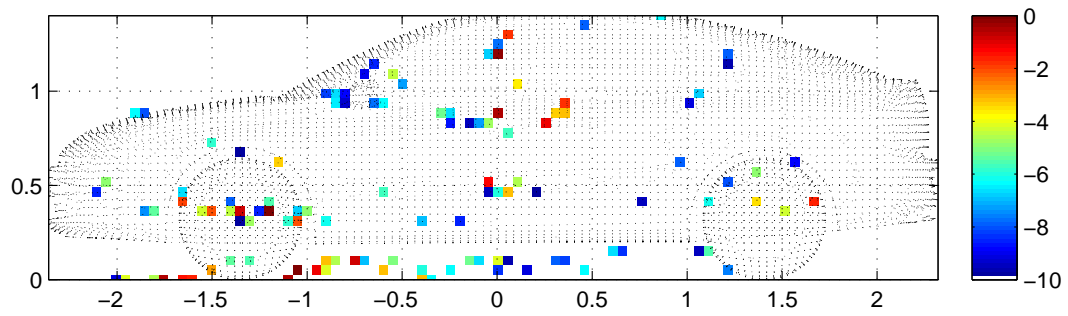
(c) DAMAS on hybrid data.



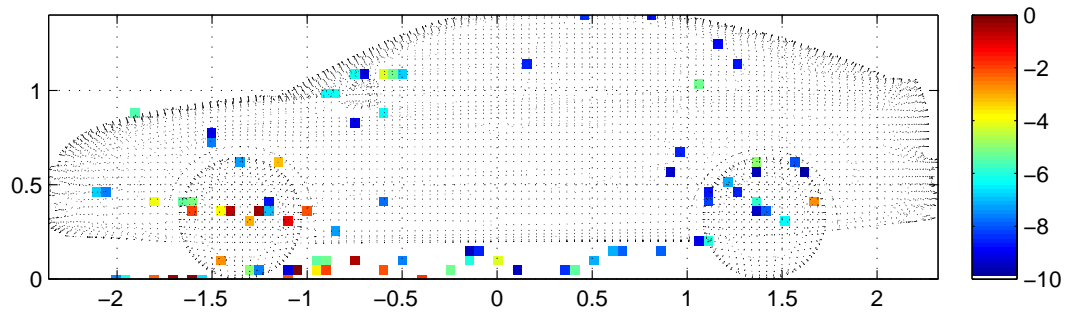
(d) DR-DAMAS on hybrid data.



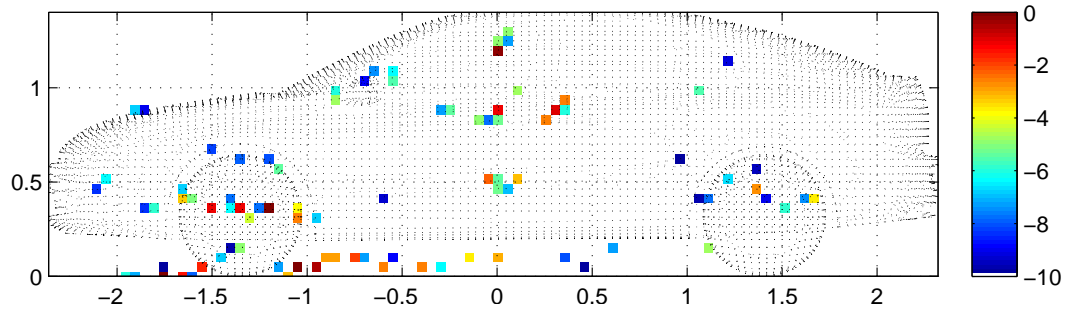
(e) CLEAN on hybrid data.



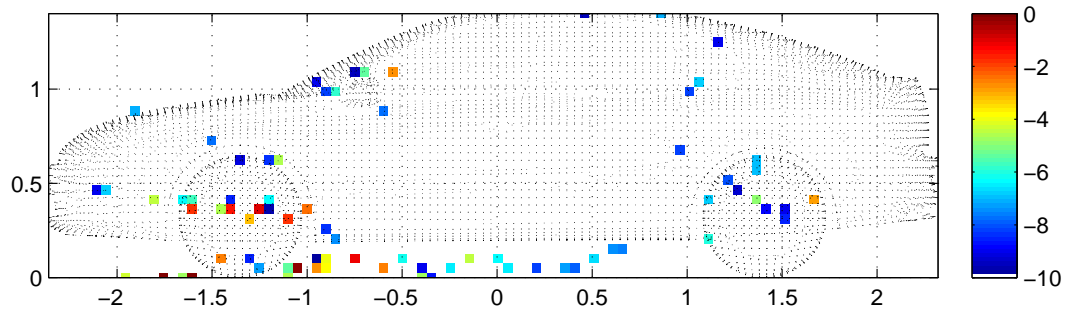
(f) SC-RDAMAS on hybrid data.



(g) SC-RDAMAS on real data



(h) SR-RDAMAS on hybrid data.



(i) SR-RDAMAS on real data

Figure 5: Results on hybrid data and on real data, imaging at 2500Hz.

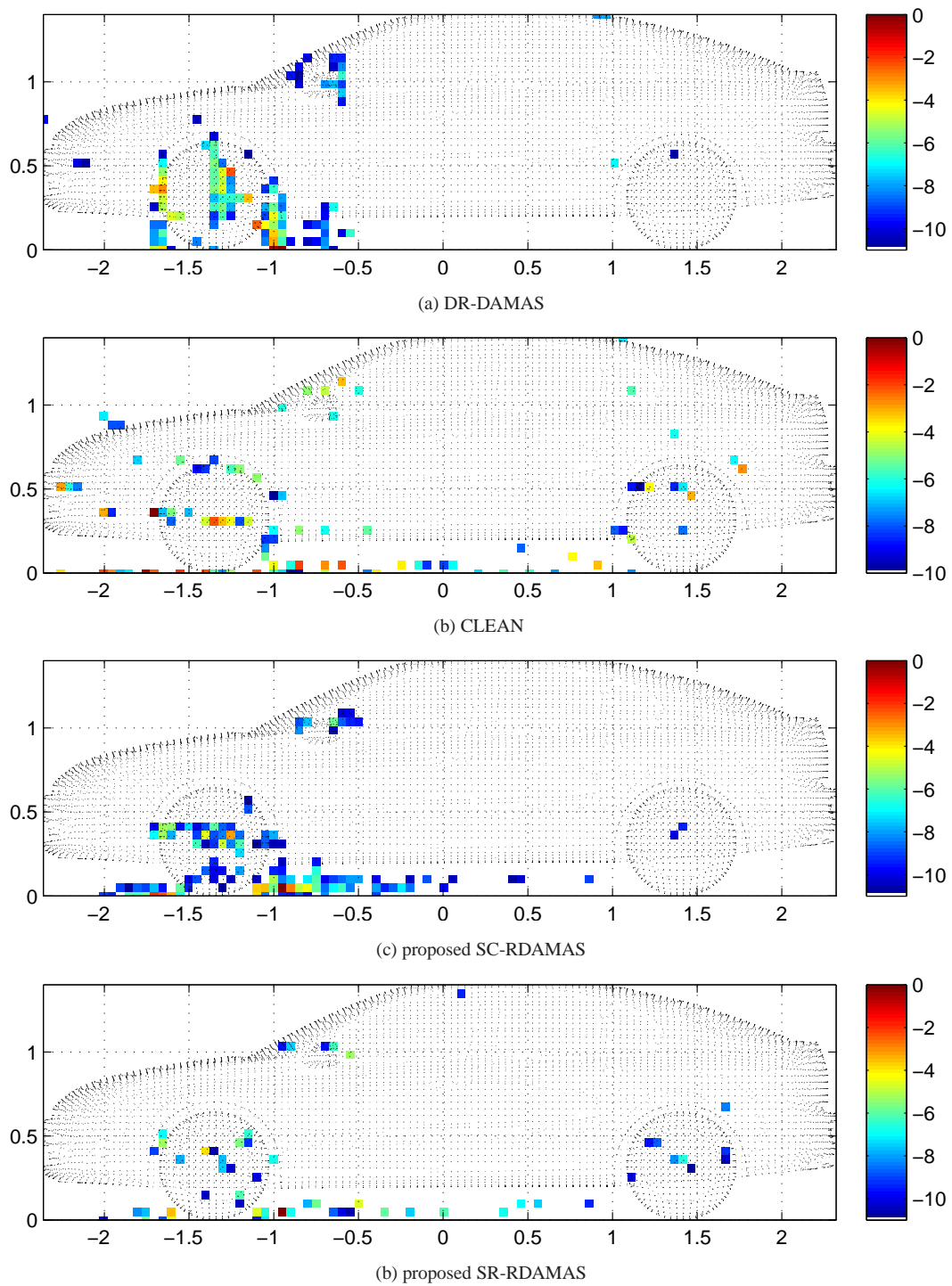


Figure 6: Wideband data over $[2400, 2600]Hz$, 10dB span